Section II

Surface Chemistry of Rh-Mo/γ-Al_2O_3: An Analysis of Surface Acidity

Research Context

In Section I, comparisons of catalyst materials centered on the significance of using a binuclear, homogeneous precursor. Substantially higher activities for CO conversion have been achieved with catalysts prepared with the *sequential* chemisorptive protocol outlined in the experimental section set forth below. Section III returns to the issue of the overall activity and selectivity of these sequentially adsorbed materials in the context of CO hydrogenation. In contrast, this section focuses on the nature of the metal-metal and metal-support interaction of significance in the synthesis of these sequentially adsorbed materials. The nature of the interactions of the Rh and Mo with the native γ-Al_2O_3 surface also influence the propensity of the catalyst, in its final form, to dehydrate first rank alcohol products produced in CO hydrogenation. This secondary, and in some cases, retrograde transformation to ethers takes place at the Lewis acid centers on the catalyst surface. Hence, the efforts set forth below focus on the nature of these Lewis acid centers, their relative strength and density across the catalyst materials which form the building blocks of the ultimate Rh-Mo/γ-Al_2O_3 system, and the effect these sites have on the alcohol dehydration potential of the materials. In order to modify their Lewis acidity, KNO_3 was used to dope the surfaces of both native Al_2O_3 and the metal-loaded samples. The KNO_3 was applied to samples using both ion exchange and incipient wetness techniques, and as a matter of course, the ultimately achievable potassium loading using these two techniques offered further insight about the nature of catalysts' surface properties as set forth in the discussion below. The most significant findings reported here, concern the interplay between the Lewis acid sites on the Al_2O_3 surface and the chemisorbing Rh precursor.

Section Abstract

This study highlights the nature of the interactions between the transition metals in the Rh-Mo/γ-Al_2O_3 system and the underlying alumina surface. The investigation was carried out in the context of exploring the retrograde dehydration to dimethyl ether of primary alcohols produced at active metal sites during CO hydrogenation. Both native γ-Al_2O_3 and Rh-Mo/γ-Al_2O_3 samples were doped with KNO_3 in an attempt to create an alkaline-metal oxide layer on the support surface which would screen alcohols from underlying Lewis acidity. The samples were characterized by microreactor-based methanol dehydration studies, analysis of infrared spectra of adsorbed pyridine, and ammonia saturation and temperature-programmed desorption. As expected, the dehydration activity of the samples was strongly correlated to their potassium loading and, hence, their Lewis acidity. More intriguing however, are the insights gained in this analysis concerning the nature of the interactions between Mo, Rh, and the Lewis acid sites on the alumina surface. Our results are consistent with the principal, suggested in the Mo/γ-Al_2O_3 literature, that our $Mo(CO)_6$ precursor interacts primarily with non-acidic hydroxyl groups on the dehydrated alumina surface. Furthermore, we provide strong evidence for the diminution of acidity brought on by the adsorption of Rh on Lewis acid sites of Mo/γ-Al_2O_3.

Introduction

Past investigations of a series of alumina-supported bimetallic combinations of Group VI and noble transition metals identified synergistic characteristics of Rh-Mo/γ-Al_2O_3 *(1,2)*. Promoting rhodium with molybdenum oxide produced a catalyst with a significantly higher propensity for the production of oxygenates in the hydrogenation of CO than could be achieved using a monometallic rhodium catalyst at both atmospheric and moderate (~1.7 MPa) pressures. Other researchers have reported oxo-selectivity and activity enhancements on silica- and alumina-supported rhodium catalysts as a consequence of molybdenum promotion *(3-6)*. Based on a combination of microreactor testing for CO hydrogenation, TEM and XPS analysis, and

H_2-chemisorption measurements, a qualitative model for the behavior of Rh in the presence of MoO_x was proposed wherein the oxidized Mo acts primarily as a textural promoter in small, bimetallic crystallites (~0.5 nm), site-isolating rhodium aggregates which would otherwise tend to sinter and agglomerate at comparable loadings. These site-isolated rhodium aggregates are thought to be primarily responsible for the oxygenate chemistry of the catalyst in the presence of synthesis gas. Larger, rhodium-rich bimetallic aggregates (~1.0 to 1.5 nm) were proposed to be primarily responsible for the dissociative adsorption of CO and subsequent hydrocarbon formation. Some infrared spectroscopic evidence in the literature *(7,8)* points to the partial oxidation of larger rhodium particles via migration of molybdenum oxide onto the surface of such larger rhodium aggregates. In contrast, Kip et al. *(3)*, in an extended study of promoted Rh/SiO_2, employing temperature programmed reduction and oxidation, transmission electron microscopy, and CO hydrogenation probe reactions, as well as infrared spectroscopic analysis, found no evidence for molybdenum oxide migration onto rhodium aggregates (as opposed to the migration demonstrated by oxides of thorium and vanadium). More recently, in a study of $Rh\text{-}Mo/SiO_2$ derived from metal-carbonyl precursors, Trunschke et al. *(6)* suggest a textural promotion role for molybdenum oxide, wherein it stabilizes smaller rhodium aggregates—identified by their signature gem-dicarbonyl infrared doublets—against sintering and agglomeration upon exposure to reaction conditions.

Upon testing the $Rh\text{-}Mo/\gamma\text{-}Al_2O_3$ catalysts at industrially relevant pressures, the oxygenated components of the product slate from CO hydrogenation shifted from predominantly methanol (MeOH), at atmospheric pressure, to predominantly dimethyl ether (DME) and ethanol (EtOH), at moderate pressures. We have ascribed the tendency to dehydrate primary alcohol products to secondary ether products to acidic features of the catalysts based on mechanistic evidence in the literature *(9-13)*. For example, Parera *(10)* suggests the straightforward mechanism detailed in Figure 1, wherein MeOH encounters a Lewis acid site on native alumina and dissociatively adsorbs onto the site, ejecting an H^+ ion onto an adjacent basic oxygen atom. The surface species

can then recombine to form the etherification products CH_3OCH_3 and H_2O. The chemistry governing Equation 1 of Figure 1 has been disputed in the literature *(12,13)*. Notably, using ^{18}O-labeled alcohols, Decanio et al. *(13)* have demonstrated that the basic oxygen in a Lewis acid-base pair can cleave the carbon-oxygen bond in the alcohol in contrast to the electrophillic attach of the alcohol function by the Lewis site. While this reaction was detected using $CH_3{}^{18}OH$, the propensity of the surface toward basic attack was found to be a function of alkyl chain length. The net products in Equation 1 are the same in either case. Hence, for the purposes of this study we have focused our efforts on characterization efforts on measuring Lewis *acidity*.

In this study, we quantify and manipulate the Lewis acidity of γ-Al_2O_3 and Rh-Mo/γ-Al_2O_3 in order to obtain insight into alcohol etherification over the Rh-Mo catalyst during hydrogenation of CO and, more importantly, the bimetallic interactions of the Rh and Mo with the alumina surface and their effect upon the acidity of the underlying support. To study the influence of surface acidity, we have synthesized a series of potassium-promoted catalysts from both native and transition-metal-loaded starting materials. The catalytic materials were then characterized using the following techniques: (i) evaluation of microreactor results for the direct dehydration of MeOH, (ii) analysis of infrared (IR) spectra of adsorbed pyridine, and (iii) analysis of ammonia saturation and temperature-programmed desorption (TPD) spectra. By mapping the surface acidity of the various transition-metal-loaded samples, intriguing evidence concerning the nature of the interaction between the transition-metal precursors and the acidic surface features of the support became apparent. The implications of this evidence on the process by which transition-metal carbonyl precursors interact with the surface of alumina during chemisorption and calcination are also discussed herein.

Methods

Catalyst Synthesis

The support common to all the samples tested in this study was γ-Al_2O_3 (American Cyanamid, BET Surface Area = 250 m^2/g). In all cases, the support was dehydrated in air at atmospheric pressure and 120 °C overnight for approximately 12 h prior to modification or testing. The dehydrated support was then used as the starting material for the series of samples synthesized in this study. The samples generated can be broadly divided into two categories: (i) doped, native alumina and (ii) doped Rh-Mo/γ-Al_2O_3.

Native alumina was doped with KNO_3 (EM Science) via two methods. In the first method, the "ion-exchange" method, three separate batches of dehydrated alumina (~3 g each) were slurried and continuously stirred for 12 h in aqueous solutions of KNO_3 with the concentrations of approximately 0.12 M, 0.24 M, and 2.40 M, respectively. These samples were subsequently dried, filtered and calcined in air at 300 °C overnight for approximately 12 h. In the second method, the "aqueous impregnation" method, two separate batches of ~3 g of dehydrated alumina were impregnated with 2.63 M and 3.0 M aqueous solutions of KNO_3 to incipient wetness (0.79 ml/g) and calcined in air at 300 °C overnight for approximately 12 h. One of the aqueous impregnation samples was then reimpregnated with the 3.0 M KNO_3 solution and calcined a second time to achieve a higher potassium loading. The second impregnation was necessary due to the solubility limit of KNO_3 and the pore volume capacity of the alumina.

In order to prepare potassium doped Rh-Mo/γ-Al_2O_3 samples, transition-metal loaded samples had to first be synthesized. Approximately 60 g of dehydrated alumina was slurried with 250 ml of anhydrous heptane (99+% pure, Aldrich). The heptane-alumina slurry was degassed by refluxing the heptane under flowing N_2 (dried and deoxygenated) for 1 h. The mixture was allowed to cool to room temperature and 11.0 g of $Mo(CO)_6$ (Strem) were added. The slurry was again brought up to reflux temperature under flowing N_2. Upon heating to reflux, the $Mo(CO)_6$

rapidly dissolved in the heptane, and almost immediately upon reaching refluxing temperature, the initially off-white alumina turned deep yellow. The color change in the alumina was associated with the chemisorption of $Mo(CO)_6$ on the support surface. IR analysis of a self-supporting wafer confirms this adsorption. The mixture was continuously stirred at reflux for 8 h, cooled to room temperature, and filtered and dried in air. The $Mo/\gamma\text{-}Al_2O_3$ material was then slurried with 250 ml of fresh anhydrous heptane. The new slurry was again degassed by refluxing under flowing N_2 for 1h and cooled to room temperature. Finally 5.0 g of $Rh(I)(CO)_2(acac)$ (Strem) were added to the slurry and again stirred and refluxed under flowing N_2 for approximately 8 h, at which time the initially cloudy, brown supernatant had cleared, and IR analysis of the liquid phase indicated that no appreciable Rh carbonyls were present. The final material was again filtered and dried in air and the resultant catalyst was mildly calcined at 120 °C overnight for approximately 12 h to both volitalize any residual heptane on the surface and oxidized the Mo and Rh.

Both the ion exchange and the aqueous impregnation methods described for the doping of alumina (*vide supra*) were employed to synthesize potassium promoted $Rh\text{-}Mo/\gamma\text{-}Al_2O_3$ samples. Interestingly, however, the ultimately achievable potassium loading for the ion-exchanged $Rh\text{-}Mo/\gamma\text{-}Al_2O_3$ was considerably lower than that achieved on doped, native alumina.

Methanol Dehydration Studies

The catalytic materials synthesized in this study have been tested for their propensity to dehydrate MeOH. In the MeOH dehydration experiments, approximately 0.15 g of sample was packed into a 5 mm I.D. Pyrex microreactor tube and loaded into a tube furnace (Lindberg 55031). In this reactor, the MeOH was fed directly to the packed bed by passing 25 cm^3/min of He carrier gas through a MeOH sparger, maintained at a constant temperature of 10 °C with a circulating temperature bath. The MeOH-saturated carrier gas was fed to the packed bed which was maintained at temperatures of 180 to 250 °C depending on the particular sample and

objectives of the reactor test. The reactor effluent was separated and analyzed by gas chromotography using a 12 ft, 1/8 in O.D. packed column containing 80 × 100 mesh Poropak T (Supelco) and a flame ionization detector to obtain conversion of MeOH to DME (or in the case of the Rh-Mo/γ-Al_2O_3 series of samples, DME, light hydrocarbons, and formaldehyde). All rate data reported in this study are for conversions of less than 10% so that differential reactor conditions can be assumed.

Pyridine Adsorption and IR Analysis

The pyridine (99+% pure C_5H_5N, Aldrich) used in this study was refluxed over excess CaH_2 for 48 h under flowing N_2 and distilled and stored on 5Å molecular sieves prior to use in the surface characterization of catalyst samples. The dried pyridine was also degassed by repeated freeze-pump-thaw cycles before dosing the surface of a sample. The sample was ground to roughly 200 × 325 mesh (~60 μm) and pressed into a self-supported wafer approximately 1.5 cm in diameter. The wafer was placed in a sealed quartz transmission infrared cell equipped with NaCl windows and 2 vacuum stopcocks for gas treatment and evacuation. The cell was then heated to 300 °C and simultaneously evacuated to approximately 3×10^{-3} Torr (1 Torr = 133.3 Pa) until the IR peaks associated with water on the wafer surface and CO_2 in the purged chamber surrounding the cell had diminished to insignificant levels. Following dehydration to 300 °C, the cell was cooled to 200 °C and the temperature was allowed to stabilize for approximately 30 min. An IR background spectrum was then collected, and all other spectra collected from the sample were referenced to this background (i.e., evacuated sample at 200 °C). Next, saturated pyridine vapor was allowed to equilibrate with the sample surface until repeated collection of IR spectra showed no increase in pyridine peak intensities (approximately 30 min). Finally, two sets of IR spectra were collected on the pyridine-saturated samples: (i) spectra for the samples in equilibrium with the saturated vapor, and (ii) spectra for the surface after the wafers had been evacuated to 3×10^{-3} Torr following pyridine dosing (evacuated for not less than 1 h). All

spectra discussed herein were recorded after 30 scans, have a resolution of 4 cm^{-1} and were collected on a Nicolet 510M Fourier Transform Infrared Spectrometer.

Ammonia Saturation and Temperature-Programmed Desorption

As an additional measure of the surface acidity of the samples examined in this study, we have collected ammonia saturation data and TPD spectra for the samples in Table 1. The ammonia used in the saturation and TPD analysis was 3.1% vol. NH_3 in a balance of He (certified, Matheson). Approximately 0.3 g of 60 × 100 mesh (~200 μm) catalyst was packed in a 9 mm I.D. quartz microreactor tube between plugs of glass wool, and the tube was placed in a tube furnace (Lindberg 55035) and put on-line with flowing He at 10 cm^3/min. The sample was allowed to equilibrate at 50 °C and was then dehydrated by ramping to 400 °C at a rate of 7 °C/min and soaking at 400 °C for 50 min under flowing He. Finally, the sample was cooled to 50 °C (chosen to minimize the effects of ambient temperature fluctuations), the carrier gas stream was switched from He to NH_3 in He, and the gas eluted from the column was monitored with a thermal conductivity detector (TCD, Gow-Mac 40-250/252). When the baseline of the chromatogram had shifted and leveled off, indicating that the column was saturated with ammonia, the carrier was switched back to pure He and the temperature was ramped form 50 to 400 °C at 7 °C/min and then soaked for 50 min at 400 °C. The temperature program naturally led to the desorption of the NH_3, and this was manifest as a peak or series of peaks in the chromatogram.

Results

K-Doped γ-Al_2O_3

Figure 2 depicts the steady-state conversion of MeOH to DME as a function of potassium loading on γ-Al_2O_3. The downward sloping trend in the data clearly indicates that as the potassium loading increases, the tendency to dehydrate MeOH is inhibited. The data shown for

8.2 and 11.9% potassium loadings resulted from samples made by the aqueous impregnation method.

The chemisorptive characterization data for this series of samples suggests that the decrease in methanol dehydration propensity with increasing potassium loading is due to a decrease in the surface acidity of the samples. Figure 3 contains two pyridine adsorption spectra: the IR absorbance of a self-supporting wafer of γ-Al_2O_3 maintained at 200 °C in a saturated atmosphere of pyridine vapor and the same wafer after the sealed IR cell has been evacuated to 3×10^{-3} Torr, following exposure to pyridine. The spectrum collected prior to evacuation contains the expected features for native γ-Al_2O_3. From the work of Parry *(14)*, the intense peak at 1453 cm^{-1}, the strong peak at 1495 cm^{-1}, and that falling in the range 1600 to 1633 cm^{-1} can be assigned to vibrational modes of pyridine coordinatively bonded to the Lewis acid sites of the surface. Parry's analysis also suggests that the broad band between 1580 and 1600 cm^{-1} is attributable to the vibrational modes of pyridine molecules physisorbed on the surface through hydrogen bonding or other dispersion forces. As expected with native γ-Al_2O_3, the concentration of acidic surface hydroxyls is insignificant as evidenced by the lack of a strong signature Brönsted peak at ~1540 cm^{-1}. Note that after the cell is evacuated, the broad peak at 1580–1600 cm^{-1} has greatly diminished, indicating that the physisorbed pyridine has desorbed from the surface. In addition, the signature Lewis acid peaks, while slightly less intense, are well resolved and still present, indicating the existence of chemisorbed pyridine which is bonded strongly to the surface.

When the same pyridine adsorption protocol and IR analysis is carried out on the 8.2 and 11.9% K-doped γ-Al_2O_3, the spectra for the evacuated samples indicate that the Lewis acid sites on the surface coordinatively bond to pyridine more weakly than on native γ-Al_2O_3. This effect is apparent in Figure 4, where the spectrum for the evacuated 11.9% K sample lacks Lewis acid signature peaks and indicates that by doping the surface with potassium, the acidity has been quashed. The spectra for the 8.2% K-doped sample demonstrate the same trend and are not shown for the sake of brevity.

The ammonia saturation and TPD results for the potassium-doped alumina samples are consistent with the premise that increasing the potassium loading leads to decreased acidity. Table 1 lists the ammonia saturation results for selected catalyst samples synthesized for this study. As the first three entries of Table 1 indicate, the calculated number of reversible acid sites interacting with NH_3 below 400 °C drops considerably for the 8.2 and 11.9% potassium samples compared to native γ-Al_2O_3. "Reversible sites" are defined here as those which desorb NH_3 during the heating cycle of the sample which includes a maximum temperature exposure of 400 °C.

The reduction in acidity with increasing potassium loading is also demonstrated in Figure 5 which depicts the TPD traces for a series of alumina samples as a function of temperature. The TPD trace for native γ-Al_2O_3 has significant fine structure above 110 °C associated with convoluted peaks representing NH_3 desorbing from surface acid sites of increasing strength. This fine structure is greatly diminished when the loading is increased to 8.2 and 11.9% potassium. For the 8.2% potassium sample, only weaker acid sites are interacting with the NH_3 below 400 °C, and such sites desorb NH_3 very early in the temperature ramp. The 11.9% potassium sample again principally desorbs ammonia below 120 °C. The sites associated with the second broad peak in the 11.9% potassium trace between 150 and 250 °C may be an artifact of the synthesis protocol of this sample which required two impregnation and calcination steps, compared to the one required to make the 8.2% potassium sample. During the second impregnation, the surface may have been inadvertently rehydrated.

K-Doped Rh-Mo/γ-Al_2O_3

Figures 6 and 7 detail the microreactor results for the K-doped Rh-Mo/γ-Al_2O_3 samples. Figure 6 contains data for samples synthesized by both the ion exchange and aqueous impregnation methods and demonstrates that as the potassium loading increases, the rate of formation of DME from MeOH diminishes. Most of downward sloping trend in DME formation

as a function potassium loading is attributable to the first four points on this figure. These points represent the samples synthesized via the ion exchange method and hence have lower potassium loadings. This section of Figure 6 is expanded in Figure 7 which shows that for the sample with a 0.090% potassium loading, the rate of formation of DME has dropped by nearly a factor of 2 compared to the untreated Rh-Mo/γ-Al_2O_3 surface.

The pyridine adsorption spectra for the transition-metal loaded samples are shown in Figures 8, 9, and 10. The spectra in Figure 8 for Mo/γ-Al_2O_3 have essentially the same features as those in Figure 3 for native alumina, indicating the presence of significant Lewis acidity on the surface of this sample. In contrast, the spectra in Figure 9, the pyridine adsorption spectra for Rh-Mo/γ-Al_2O_3, have features reminiscent of a highly K-doped alumina. While Lewis acid signature peaks are present when the Rh-Mo/γ-Al_2O_3 sample is in equilibrium with pyridine vapor, these same peaks vanish when the sample is evacuated. Here, the process of chemisorbing the rhodium and oxidizing the catalyst has reduced the acidity of the surface. In Figure 10, which depicts the spectra for K-doped Rh-Mo/γ-Al_2O_3, the evacuated sample again lacks Lewis acid signature peaks. The spectrum for the evacuated, doped sample is essentially unchanged from that of the undoped sample.

Ammonia saturation and TPD results are presented in Table 1 and Figures 11 and 12. The results presented in Table 1 indicate that the acid amount of sites interacting with NH_3 increases markedly upon addition of 2.5% molybdenum to the alumina surface. This increase can be related to the stoichiometry of the metals present on the surface, as will be discussed below. Figure 12, the TPD traces for the series of doped Rh-Mo/γ-Al_2O_3 samples, suggests that while the total acid amount of reversible sites may be unchanged, the distribution of reversible sites shifts toward sites which interact *more* strongly with ammonia after the surface has been doped with potassium. This effect may be associated with both the ion exchange protocol used to synthesize these samples which may have rehydrated the surface and the relative basicity of NH_3 compared to pyridine.

Discussion

Past efforts to functionalize the alumina surface of rhodium-based catalysts focused on the role hydroxyl sites play in the sintering of monometallic, supported catalysts in high-temperature reactive environments. Yates et al. *(15-17)*, in a series of investigations in 1991, demonstrated that in the presence of CO above 600K, Rh(0) is oxidized on fully or partially hydroxylated alumina to form rhodium gem-dicarbonyl, $Rh(I)(CO)_2$, by the following surface reaction:

$$\frac{1}{x}\,Rh_x^0 + Al-OH + 2\,CO_{(g)} \longrightarrow (Al-O^-)Rh^I(CO)_2 + \frac{1}{2}\,H_{2(g)}$$

Yates, as well as other researchers *(18-21)*, contend that the formation of rhodium gem-dicarbonyl is correlated with rhodium's surface mobility and tendency to sinter and deactivate at high temperature. To combat this phenomenon, Yates first dehydroxylates the surface by evacuating $Rh/\gamma\text{-}Al_2O_3$ at high temperature (475–900 K), and he later explores functionalizing the surface using both trimethyl silane and potassium (from K_2CO_3) to cap nucleophillic surface oxygen atoms and thus stabilize rhodium atoms in a highly dispersed array.

In contrast to the functionalization efforts of Yates, the bimetallic materials synthesized in this study are thought to employ molybdenum, in the form of highly dispersed molybdenum anhydrides, to stabilize a high dispersion of rhodium. The efforts to potassium dope the surface of both the metal-loaded and native support are aimed, in part, at addressing the reactivity of the underlying alumina and stemming its retrograde dehydration activity. The approach is meant to synthesize an alkaline-metal oxide layer on the alumina surface which effectively screens primary alcohol products of hydrogenation from the adsorptive sites of the support—believed here to be the Lewis acid-base pair sites of the support. Our microreactor results demonstrate, as expected, that the potassium loading is directly correlated with dehydration activity for both native alumina and the $Rh\text{-}Mo/\gamma\text{-}Al_2O_3$. More intriguing, however, is the insight that can be

drawn from this study about the nature of transition metal chemisorption on the alumina surface during deposition from metal-carbonyl precursors.

Transition Metal Chemisorption Chemistry

The chemisorptive characterization of the samples with pyridine and ammonia supports our contention that the Lewis acid-base pairs play a key role in the dehydration mechanism, and the results are as expected for native alumina. The pyridine adsorption spectra in Figure 8 indicate that after the chemisorption of Mo subcarbonyl on the alumina surface and the mild oxidation of this Mo/γ-Al_2O_3 sample, the surface acidity of the material is still significant. This result is in agreement with the work of Burwell and Brenner *(22,23)*, which suggests that $Mo(CO)_6$ chemisorbs on alumina at hydroxyl sites rather than Lewis acid sites. If, upon oxidation of the material, the Mo subcarbonyl reacts with O_2 in the gas phase, the underlying Lewis acid sites of the support are left unmolested. The remaining Mo/γ-Al_2O_3 would have the acid sites associated with the underlying support and perhaps Lewis acid sites associated with the molybdenum anhydride centers on the surface. Hence the spectra in Figure 8 indicate that considerable Lewis acidity is present on the surface of the 2.5% Mo/γ-Al_2O_3. Because the pyridine adsorption technique is not quantitative, however, the increase in the acid amount, or number of pyridine-sensitive sites, cannot be accurately determined from the IR peak intensities given the degree of surface roughness in the self-supporting wafers used in this experiment.

Since the pyridine adsorption and IR analysis provided no quantitative measure of acid amount, we were motivated to use an adsorptive technique that could track the total amount of basic probe molecule adsorbed, namely NH_3 saturation and TPD. Upon examination of the second column of Table 1, the total ammonia adsorption of the samples tested, a jump in total acidity of the surface is evident when the results for native alumina and Mo/γ-Al_2O_3 are compared. When the loading of Mo is increased from 2.5% to 3.4% in the 2.8% Rh–3.4% Mo sample, the total NH_3 capacity remains fairly constant. Essentially, the increase in Mo loading

and, hence, the number of Lewis acid centers is offset by the interaction of Rh with the surface and its titration of some of the acid sites present.

The spectrum for the evacuated sample in Figure 9, depicting the pyridine adsorption spectra for Rh-Mo/γ-Al_2O_3, lacks Lewis signature peaks. This indicates that the process of chemisorbing the rhodium onto the Mo/γ-Al_2O_3 material diminishes or otherwise weakens the acid sites on Mo/γ-Al_2O_3. It is not surprising, then, that Figure 10 looks indistinguishable, within experimental uncertainty, from Figure 9. The addition of potassium to the surface of Rh-Mo/γ-Al_2O_3 has no effect on the majority of acid sites sensitive to pyridine adsorption since these sites have already been weakened or eliminated by the presence of rhodium. This ameliorating effect of chemisorbed rhodium on the final acidic character of the Mo/γ-Al_2O_3 is also the key to (i) interpreting the microreactor results of Figure 7 and (ii) the observation in the synthesis of the materials that the ultimate potassium loading achievable on Rh-Mo/γ-Al_2O_3 using the ion exchange method is only a fraction of that for native alumina (as high as 3%) when both are exposed to the same concentration of KNO_3. The majority of the acidic character typically available for MeOH dehydration and available to interact with potassium cations has already been eliminated by chemisorbing rhodium.

The relation between the transition-metal loading and the acidity of the surface of the materials in this study can be tracked in a self-consistent fashion. On native alumina, the ammonia saturation data in Table 1 suggests that the amount of ammonia adsorbing sites is approximately 2450 μmoles/g. In Peri's model for the surface of dehydrated γ-Al_2O_3 *(24)* , the hydroxyl site density is approximately 8 to 12 hydroxyl sites per 100 $Å^2$. If we assume that (i) the MoO_x is present as the surface molybdate $Mo(VI)O_4$ (see Figure 13), as XPS analysis indicates *(1)* and Raman spectroscopic investigations by Stencel et al. *(25)* and Wachs and coworkers *(26-29)* suggest, (ii) the Mo has interacted with 2 hydroxyl sites per atom of Mo in chemisorbing and oxidatively binding to the surface, and (iii) each Mo center acts as a Lewis acid site in the presence of NH_3 which can adsorb 2 NH_3 molecules per Mo, then the

stoichiometry on the 2.5% Mo/γ-Al_2O_3 sample suggests that it should adsorb approximately 2910 μmoles/g of NH_3. This simply calculated value deviates by only 3% from the experimentally measured NH_3 capacity on the 2.5% Mo/γ-Al_2O_3, as reported in Table 1. In proceeding to consider the expected acid character of the 2.8% Rh-3.4% Mo/γ-Al_2O_3, an adjustment must be made for the increase in Mo loading. Considering first only the influence of the Mo. Based on the assumptions above, the 2.8% Rh-3.4% Mo sample would be expected to adsorb approximately 3010 μmoles/g. If (i) the Rh present on the surface after oxidation of the catalyst is present as Rh(III), as XPS analysis indicates *(1)*, (ii) the rhodium oxide screens 3 Lewis acid sites of the support per Rh atom, and (iii) each Rh atom is again capable of adsorbing 2 NH_3 molecules, then the implied stoichiometry suggests that the 2.8% Rh–3.4% Mo/γ-Al_2O_3 should have an NH_3 capacity of 2738 μmoles/g. This value accounts for 96% of the NH_3 capacity measured experimentally. These results provide a systematic basis for interpreting the experimental observation that the presence of the Rh diminishes at least part of the acidity present on Mo/γ-Al_2O_3.

The final issue which must be addressed in considering the adsorptive behavior of the transition-metal loaded samples considered in this study concerns the difference in their adsorptive behavior in the presence of ammonia versus pyridine. The evacuated pyridine IR spectrum in Figure 9 for the Rh-Mo/γ-Al_2O_3 sample was similar to that of highly potassium-doped native alumina, yet the NH_3 saturation data of Table 1 suggest that the acid amount of the Rh-Mo sample is considerably larger than that of, say, doped 8.2% K on alumina sample. First, the pyridine adsorption study provided no measure of acid amount—technically, the acid *strength* of the Rh-Mo sample is comparable to that of highly doped alumina as measured by pyridine adsorption. Second, the relative tendency of NH_3 and pyridine to coordinate with transition-metal centers is strongly dependent on the π^*-backbonding ability, and hence, the oxidation state, of the transition-metal center. Shepherd and Taube *(30)* have calculated the relative ligand exchange rates for NH_3 and pyridine with $[(NH_3)_5RuOH_2]^{2+}$ and

$[(NH_3)_5RuOH_2]^{3+}$, wherein the H_2O coordination site was replaced. In their study, Shepherd and Taube calculate that for Ru^{2+}, the affinity ratio of pyridine to NH_3 was approximately 2:1, and the greater affinity for pyridine resulted from the ~ 5.8 kcal/mol relative contribution to the free energy of association due to backbonding to the pyridine. In contrast, for the Ru^{3+} which was assumed to have no net backbonding to the pyridine, the pyridine to NH_3 affinity ratio was approximately 1:4 (1:24 after accounting for a statistical factor of six in the case of NH_3). In this study, the molybdenum and rhodium—like the Ru^{3+} of Shepherd and Taube's work—are present in a highly oxidized state prior to reduction. Hence, sites sensitive to strong NH_3 adsorption on the Rh-Mo and Mo on γ-Al_2O_3 surface may not bond as strongly to pyridine, and the adsorption results for NH_3 and pyridine should be expected to quantitatively differ.

Conclusions

The results presented for the series of K-doped alumina and Rh-Mo/γ-Al_2O_3 samples synthesized in this study demonstrate that the MeOH dehydration propensity of these materials can be quantified and manipulated. This dehydration propensity has been correlated to the strength and amount of Lewis acid sites on the surface through analysis of the IR spectra of adsorbed pyridine and the NH_3 saturation and TPD data. The IR spectra of adsorbed pyridine and the NH_3 saturation and TPD data on the Rh-Mo/γ-Al_2O_3 samples show that addition of rhodium diminishes surface acidity of Mo/γ-Al_2O_3. This amelioration of acidity is evidenced by the observation that less than 6 wt% potassium doping is required on the Rh-Mo catalyst to completely quash the DME activity compared to more than 12 wt% on native γ-Al_2O_3 at temperatures of up to 250 °C. Furthermore, the chemisorptive characterization of the transition-metal loaded samples synthesized in this investigation is consistent with the contention of Burwell and Brenner *(22,23)* that the $Mo(CO)_6$ interacts primarily with hydroxyl sites on the surface of the alumina. While the chemisorbing molybdenum subcarbonyls may not materially alter the Lewis acidity of the underlying support, such adsorbed and oxidized molybdenum centers seem to function as Lewis acid sites in the presence of NH_3. The Lewis acid character of

the Mo centers is suggested by the dramatic jump in NH_3 capacity upon addition of Mo to the alumina surface. The process of chemisorbing and oxidizing a second, active transition metal from $Rh(I)(CO)_2(acac)$ leads to a dramatic reduction in the strength of the Lewis acid sites on the surface and diminishes the number of sites which actively adsorb NH_3. Additional chemisorptive characterization of transition-metal loaded samples is underway, and such studies are hoped to add more conclusive evidence to the stoichiometric arguments presented in the discussion section herein.

Acknowledgments

Helpful discussions with Dr. Alison M. A. Bennett and her assistance with pyridine pretreatment in connection with our pyridine adsorption studies are acknowledged with thanks. Support for this research was provided by the Pittsburgh Energy and Technology Center under the auspices of the Department of Energy University Coal Research Program, Grant No. DE-F622-90PC90291.

References

1. Foley, H. C., Hong, A. J., Brinen, J. S., Allard, L. F. and Garratt-Reed, A. J., *Appl. Catal.*, **61**, 351 (1990).
2. Te, M., Lowenthal, E. E. and Foley, H. C., *J. Catal.*, **146**, 591 (1994).
3. Kip, B. J., Hermans, E. G. F., van Wolput, J. H. M. C., Hermans, N. M. A., van Grondelle, J. and Prins, R., *Appl. Catal.*, **35**, 109 (1987).
4. Trunschke, A., Ewald, H., Gutschick, D., Miessner, H., Skupin, M., Walther, B. and Böttcher, H.-C., *J. Mol. Cat.*, **56**, 95 (1989).
5. Trunschke, A., Ewald, H., Miessner, H., Fukuoka, A., Ichikawa, M. and Böttcher, H.-C., *Mat. Chem. Phys.*, **29**, 503 (1991).
6. Trunschke, A., Ewald, H., Miessner, H., Marengo, S., Martinengo, S., Pinna, F. and Zanderighi, L., *J. Mol. Cat.*, **74**, 365 (1992).

7. Wardinsky, M. D. and Hecker, W. C., *J. Phys. Chem.*, **92**, 2602 (1988).

8. Decanio, E. C. and Storm, D. A., *J. Catal.*, **132**, 375 (1991).

9. Jain, J. R. and Pillai, C. N., *J. Catal.*, **9**, 322 (1967).

10. Parera, J. M. and Figoli, N. S., *J. Catal.*, **14**, 303 (1969).

11. Padmanabhan, V. R. and Eastburn, F. J., *J. Catal.*, **24**, 88 (1972).

12. Knözinger, H., Kochloefl, K. and Meye, W., *J. Catal.*, **28**, 69 (1973).

13. Decanio, E. C., Nero, V. P. and Bruno, J. W., *J. Catal.*, **135**, 444 (1992).

14. Parry, E. P., *J. Catal.*, **2**, 371 (1963).

15. Ballinger, T. H. and Yates, J. T., Jr., *J. Phys. Chem.*, **95**, 1694 (1991).

16. Paul, D. K. and Yates, J. T., Jr., *J. Phys. Chem.*, **95**, 1699 (1991).

17. Zaki, M. I., Ballinger, T. H. and Yates, J. T., Jr., *J. Phys. Chem.*, **95**, 4028 (1991).

18. Solymosi, F. and Pásztor, M., *J. Phys. Chem.*, **89**, 4789 (1985).

19. Solymosi, F. and Pásztor, M., *J. Phys. Chem.*, **90**, 5312 (1986).

20. Zaki, M. I., Kunzmann, G., Gates, B. C. and Knözinger, H., *J. Phys. Chem.*, **91**, 1486 (1987).

21. Wong, C. and McCabe, R. W., *J. Catal.*, **119**, 47 (1989).

22. Brenner, A. and Burwell, R. L., Jr., *J. Catal.*, **52**, 353 (1978).

23. Burwell, R. L. and Brenner, A., *J. Mol. Cat.*, **1**, 77 (1975).

24. Peri, J. B., *J. Phys. Chem.*, **69**, 231 (1965).

25. Stencel, J. M., Makovsky, L. E., Sarkus, T. A., De Vries, J., Thomas, R. and Moulin, J. A., *J. Catal.*, **90**, 314 (1984).

26. Chan, S. S., Wachs, I. E., Murrell, L. L., Wang, L. and Hall, W. K., *J. Phys. Chem.*, **88**, 5831 (1984).

27. Hardcastle, F. D. and Wachs, I. E., *J. Raman Spectrosc.*, **21**, 683 (1990).

28. Williams, C. C., Ekerdt, J. G., Jehng, J.-M., Hardcastle, F. D. and Wachs, I. E., *J. Phys. Chem.*, **95**, 8791 (1991).

29. Vuurman, M. A. and Wachs, I. E., *J. Phys. Chem.*, **96**, 5008 (1992).

30. Shepherd, R. E. and Taube, H., *Inorg. Chem.*, **12**, 1392 (1973).

Table Caption

Table 1. Ammonia Saturation Measurements Reflecting Surface "Acid Amount"

Sample	Reversible[(a)] NH_3 Adsorption µmoles/g sample	Total NH_3 Adsorption µmoles/g sample
γ–Al_2O_3 (American Cyanimid)	594 ± 58	2450 ± 66
8.2% K on γ–Al_2O_3	374 ±37	2270 ± 75
11.9% K on γ–Al_2O_3	349 ± 33	3080 ± 133
2.5% Mo on γ–Al_2O_3	726 ± 71	2820 ± 83
2.8% Rh – 3.4% Mo on γ–Al_2O_3	764 ± 71	2850 ± 75
2.8% Rh – 3.4% Mo on γ–Al_2O_3; 0.03% K[(b)]	722 ± 66	2570 ± 62
2.8% Rh – 3.4% Mo on γ–Al_2O_3; 0.08% K[(b)]	747 ±71	2760 ± 75

(a) Reversible sites are defined as those NH_3–sensitive acid sites which desorb NH_3 upon heating to 400 °C.

(b) The 2.8% Rh – 3.4% Mo on γ–Al_2O_3 sample was used as the starting material for these potassium-doped catalysts. While elemental analysis was used to determine the potassium content, no analysis of transition metal content was conducted following the ion-exchange protocol.

Table 1. Ammonia Saturation Measurements Reflecting Surface "Acid Amount"

Figure Captions

Figure 1. Methanol Dehydration Mechanism on Alumina, Adapted from Parera, J. M. and Figoli, N. S., *J. Catal.*, **14**, 303 (1969)

Figure 2. Steady-State Conversion of Methanol to Dimethyl Ether as a Function of Potassium Loading on γ-Al_2O_3

Figure 3. Pyridine Adsorption Spectra: Native γ-Al_2O_3

Figure 4. Pyridine Adsorption Spectra: Potassium-Doped γ-Al_2O_3, 11.9% by Weight

Figure 5. Ammonia Temperature Programmed Desorption for Series of Doped Alumina Samples

Figure 6. Dimethyl Ether Formation as a Function of Potassium Loading on 2.8% Rh-3.4% Mo/γ-Al_2O_3

Figure 7. Dimethyl Ether Formation as a Function of Potassium Loading for Rh-Mo/γ-Al_2O_3 Samples Doped via Ion Exchange

Figure 8. Pyridine Adsorption Spectra: 2.5% Mo/γ-Al_2O_3

Figure 9. Pyridine Adsorption Spectra: 2.8% Rh-3.4% Mo/γ-Al_2O_3

Figure 10. Pyridine Adsorption Spectra: Potassium-Doped Rh-Mo/γ-Al_2O_3, 0.03% by Weight

Figure 11. Ammonia Temperature Programmed Desorption Tracing Acidity from Native Alumina to Final Bimetallic Catalyst

Figure 12. Ammonia Temperature Programmed Desorption for Doped Rh-Mo/γ-Al_2O_3 Series

Figure 13. $Mo(VI)O_4$ Surface Species Adapted From Stencel, J. M. et al., *J. Catal.*, **90**, 314 (1984)

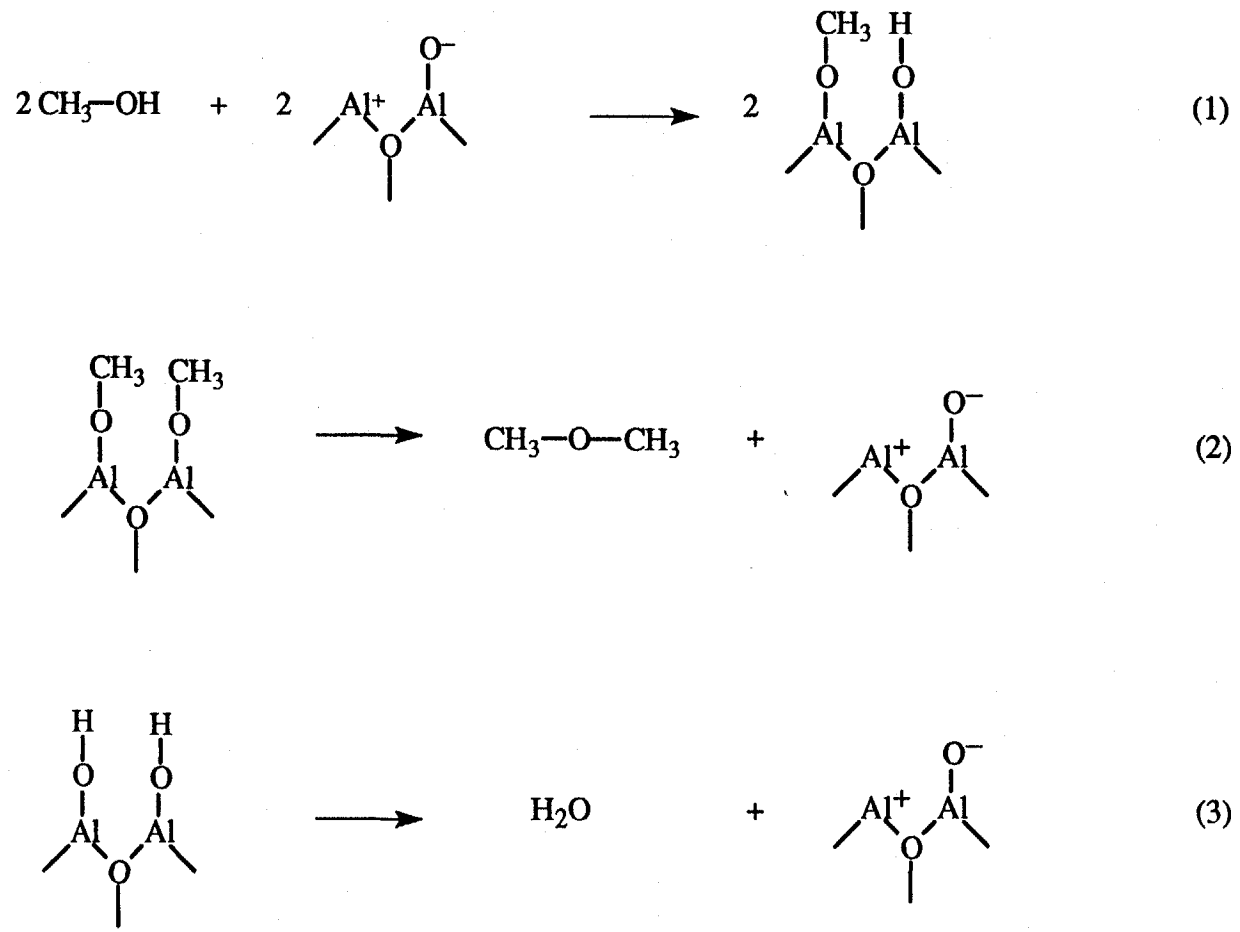

Figure 1. Methanol Dehydration Mechanism on Alumina, Adapted from Parera, J. M. and Figoli, N. S., J. Catal., 14, 303 (1969)

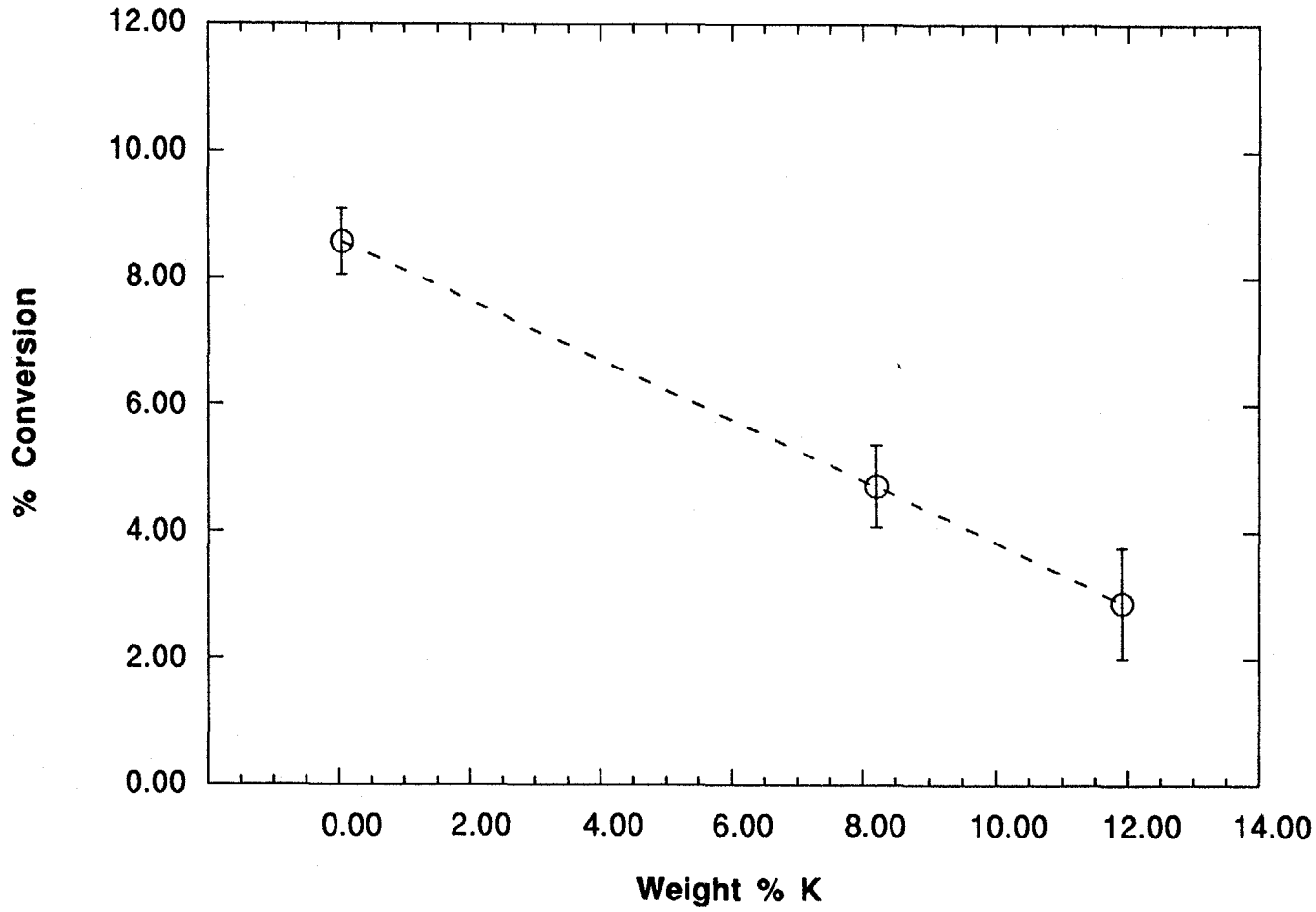

Figure 2. Steady-State Conversion of Methanol to Dimethyl Ether as a Function of Potassium Loading on γ-Al_2O_3

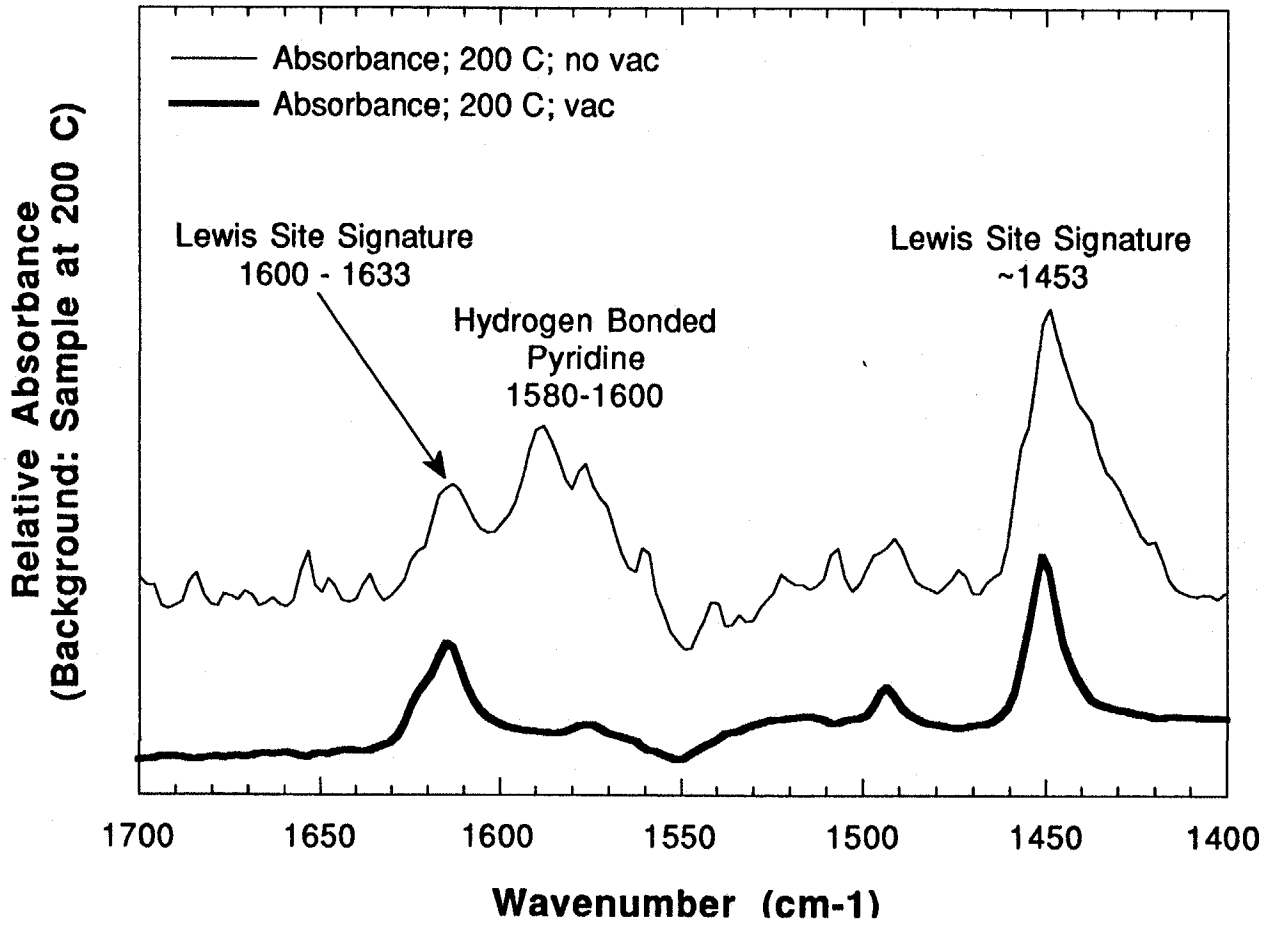

Figure 3. Pyridine Adsorption Spectra: Native γ-Al_2O_3

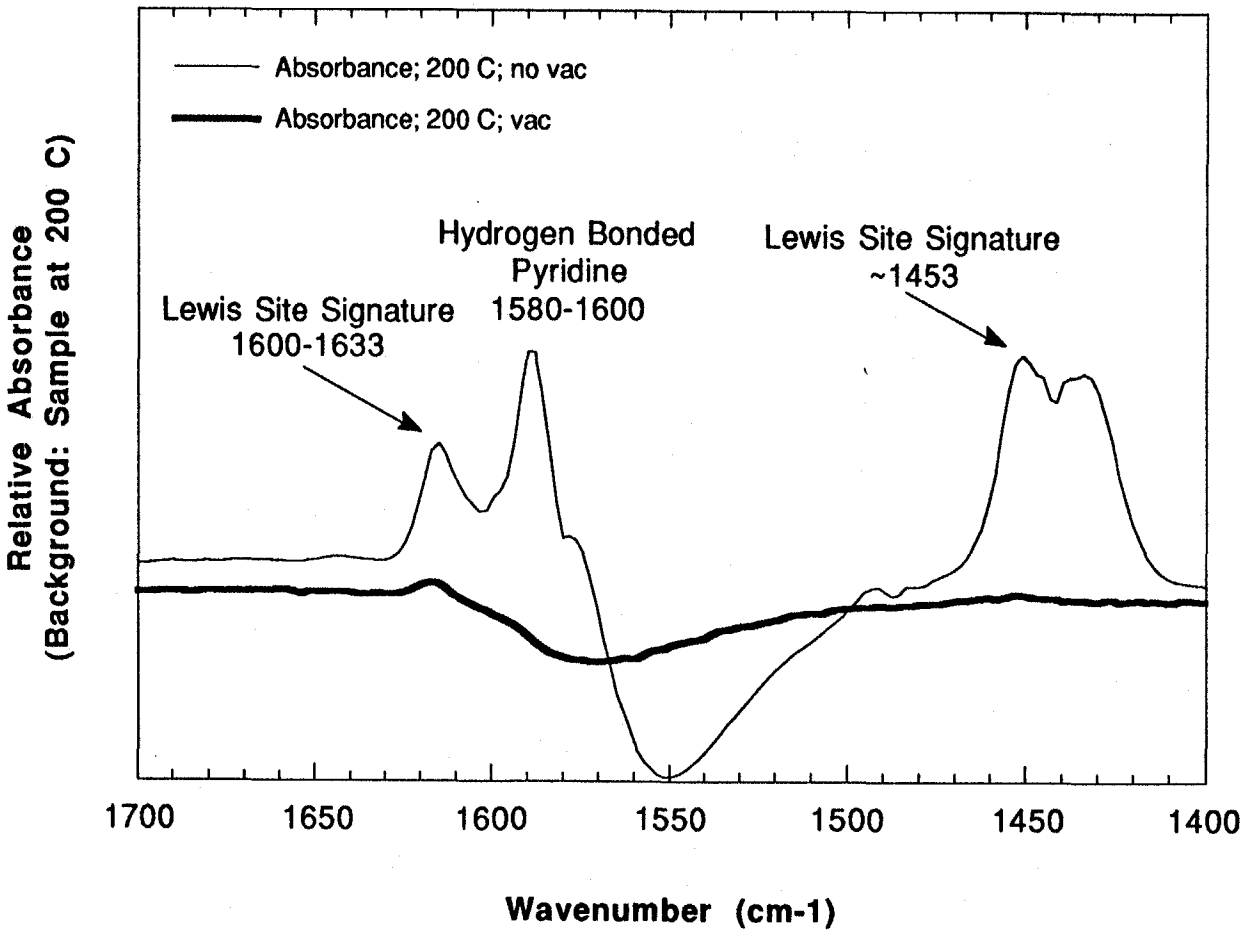

Figure 4. Pyridine Adsorption Spectra: Potassium-Doped γ-Al_2O_3, 11.9% by Weight

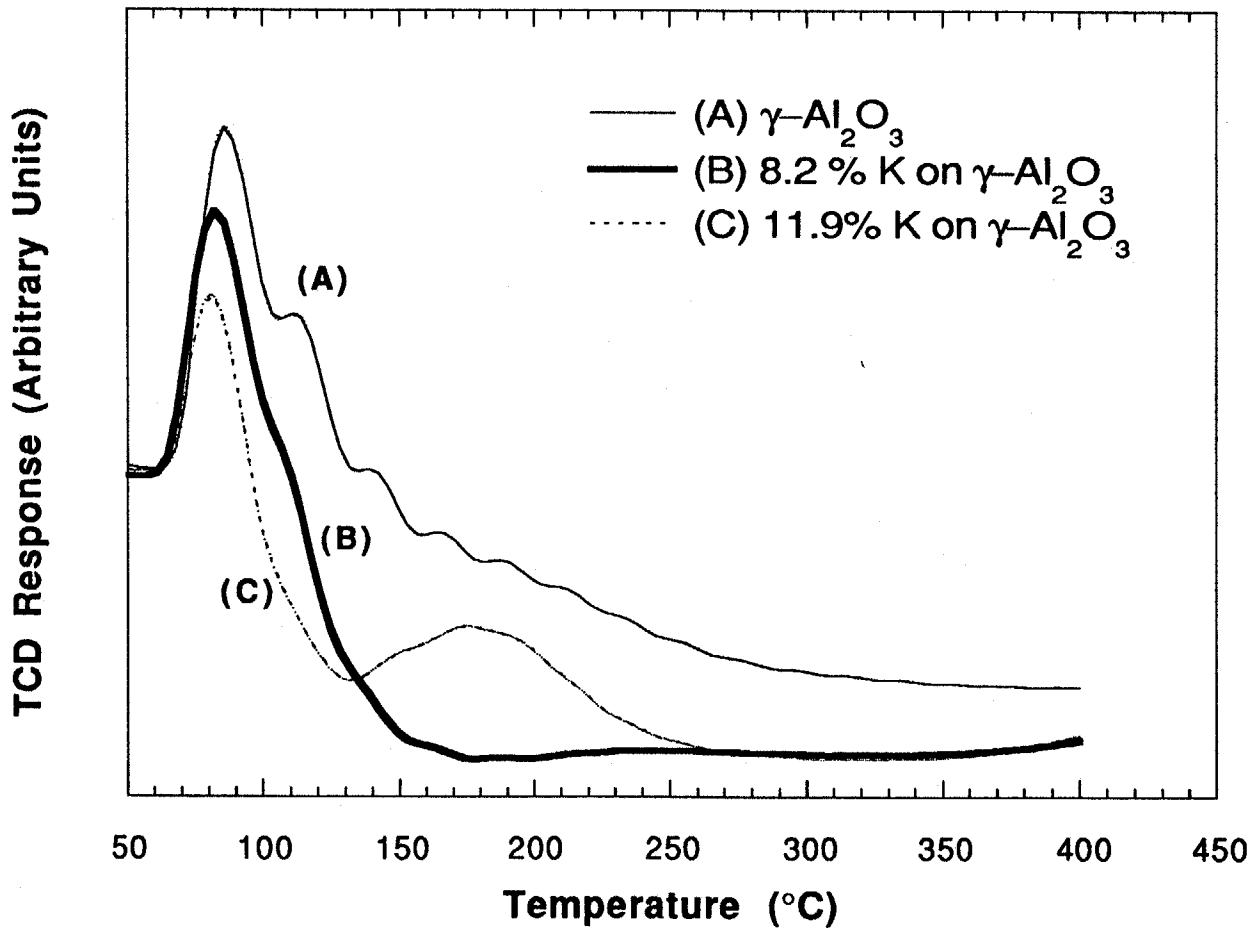

Figure 5. Ammonia Temperature Programmed Desorption for Series of Doped Alumina Samples

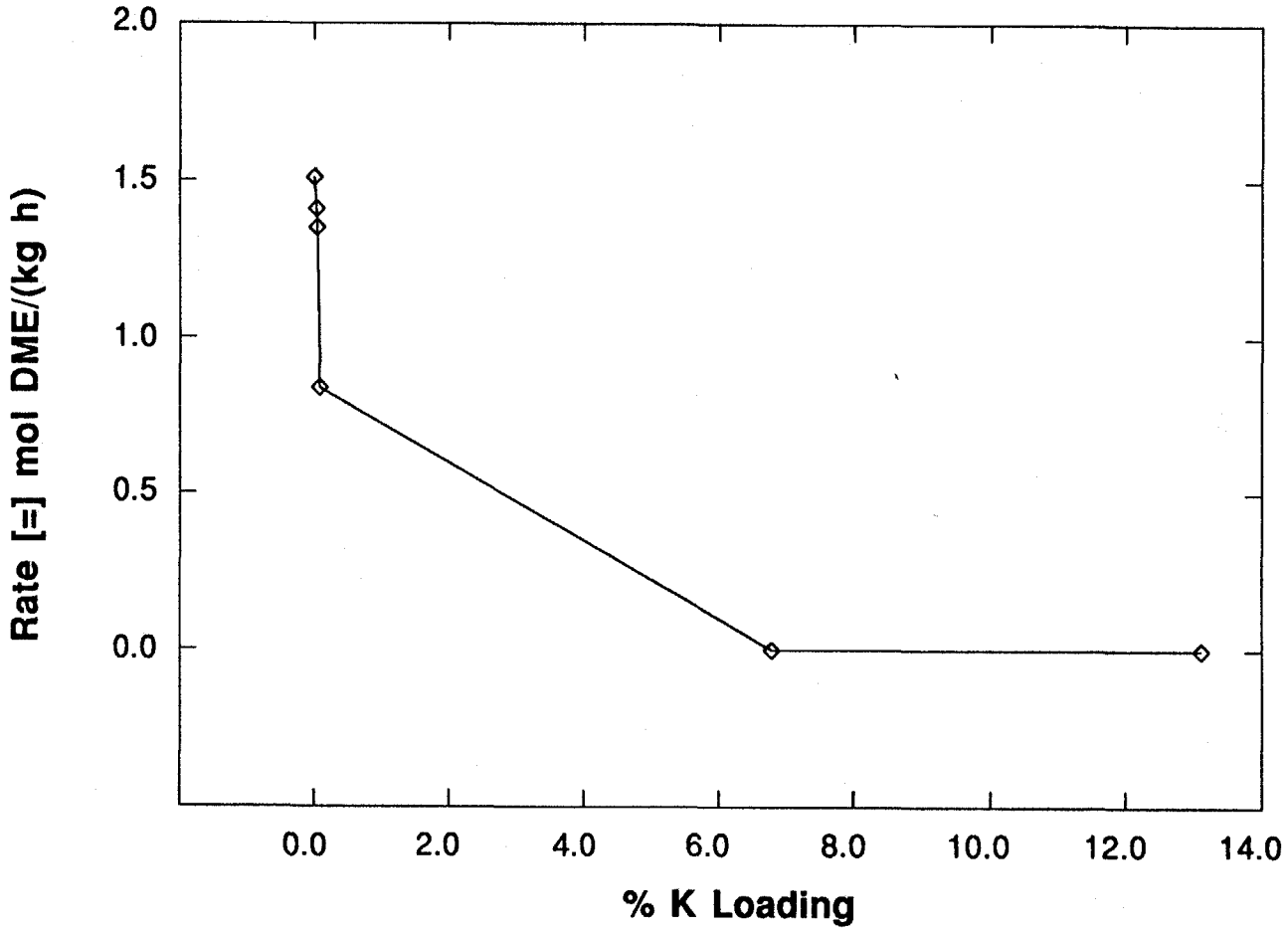

Figure 6. Dimethyl Ether Formation as a Function of Potassium Loading on 2.8% Rh-3.4% Mo/γ-Al_2O_3

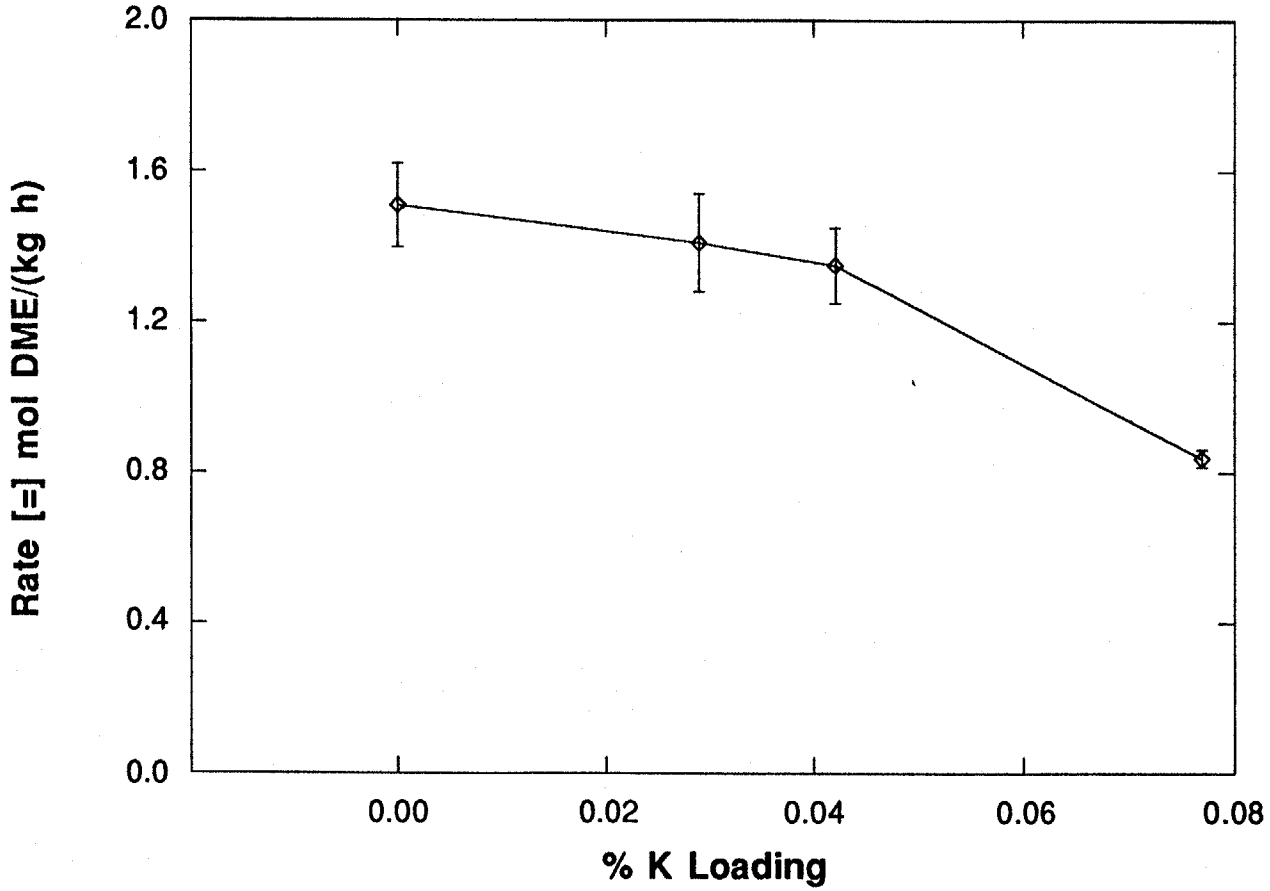

Figure 7. Dimethyl Ether Formation as a Function of Potassium Loading for Rh-Mo/γ-Al_2O_3 Samples Doped via Ion Exchange

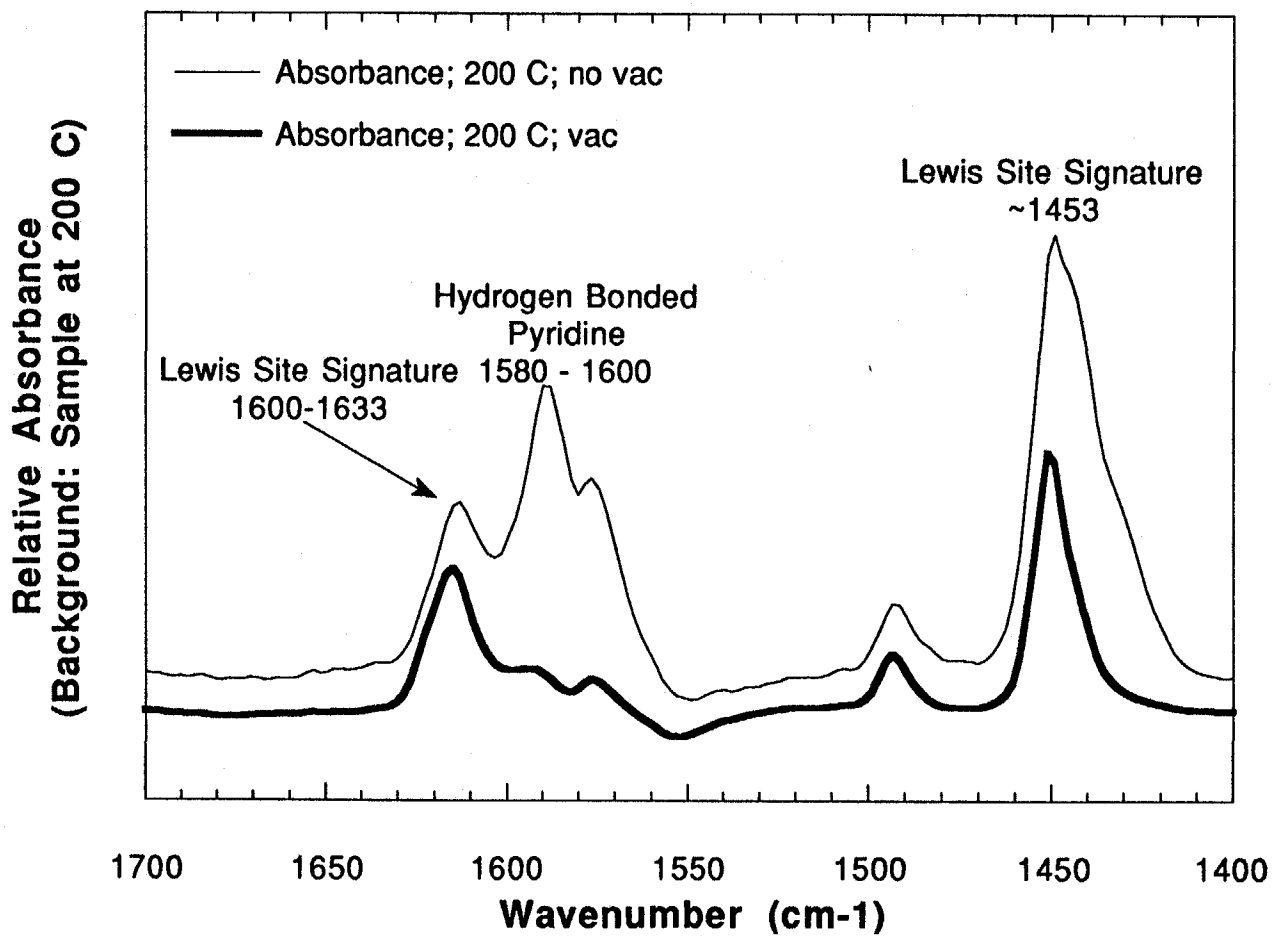

Figure 8. Pyridine Adsorption Spectra: 2.5% Mo/γ-Al_2O_3

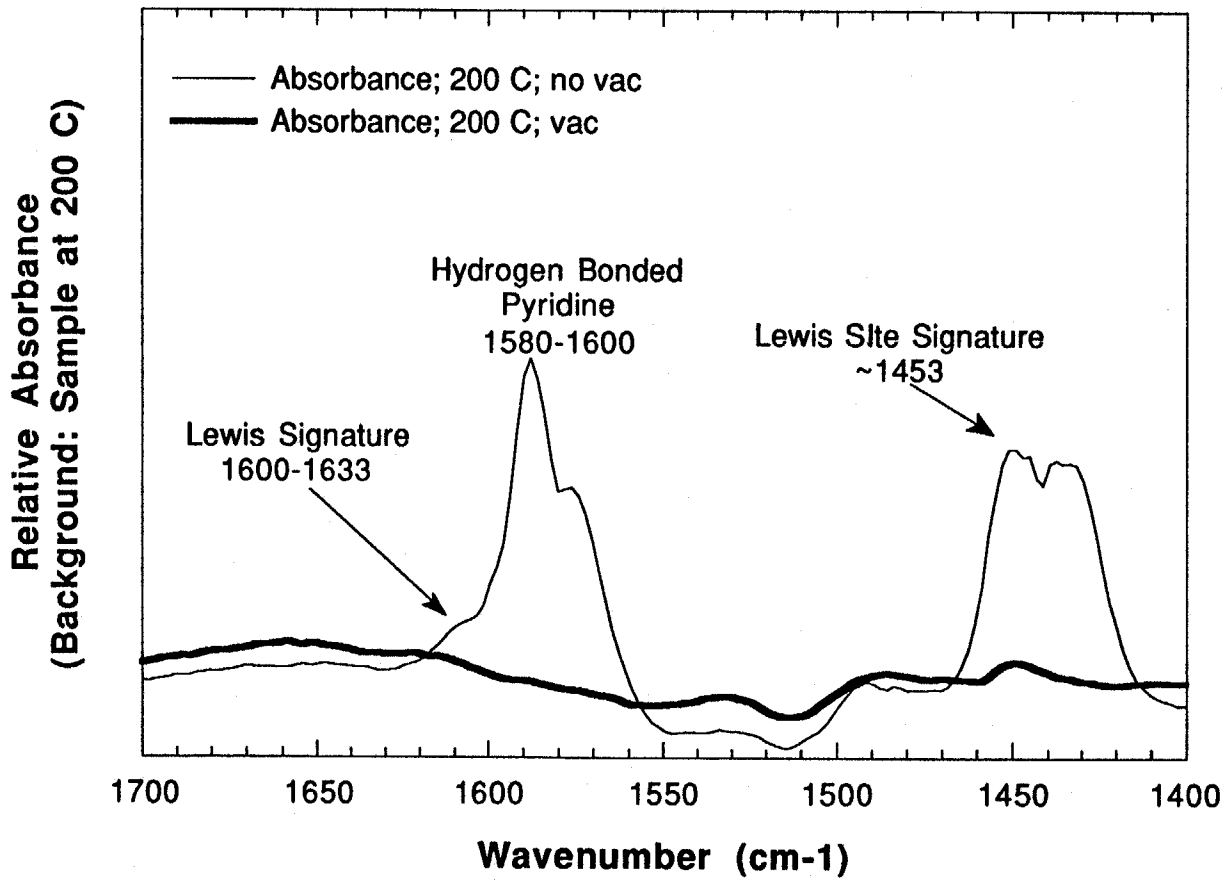

Figure 9. Pyridine Adsorption Spectra: 2.8% Rh-3.4% Mo/γ-Al_2O_3

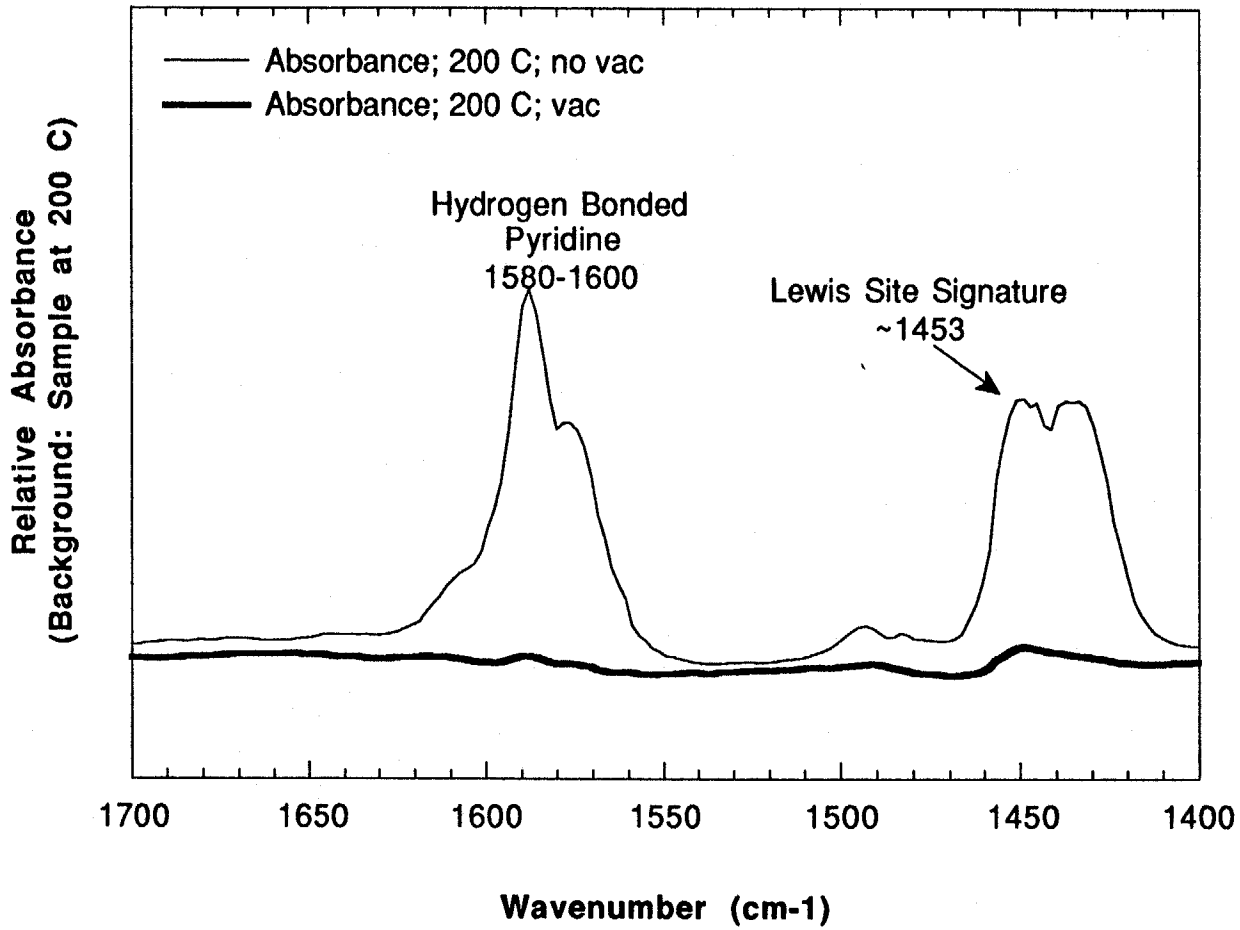

Figure 10. Pyridine Adsorption Spectra: Potassium-Doped Rh-Mo/γ-Al_2O_3, 0.03% by Weight

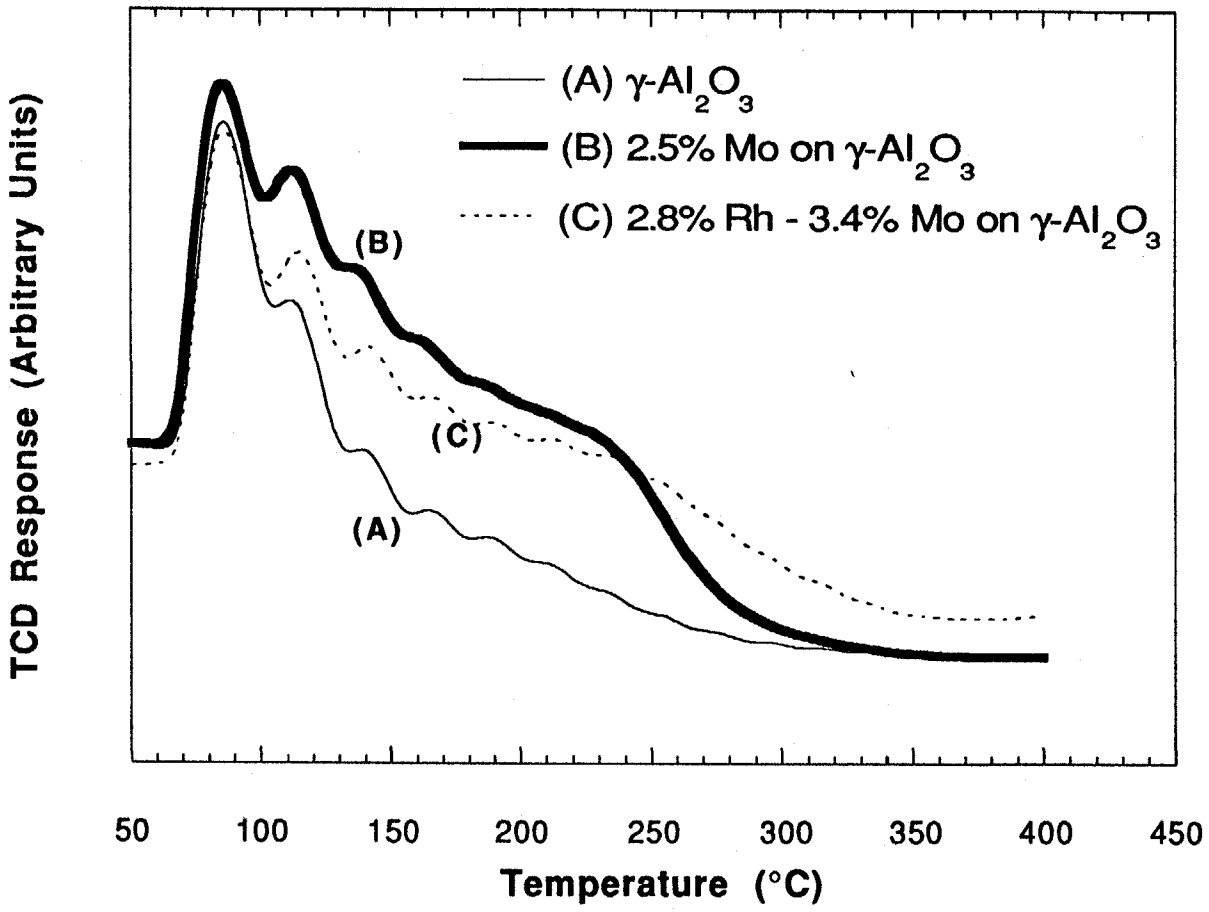

Figure 11. Ammonia Temperature Programmed Desorption Tracing Acidity from Native Alumina to Final Bimetallic Catalyst

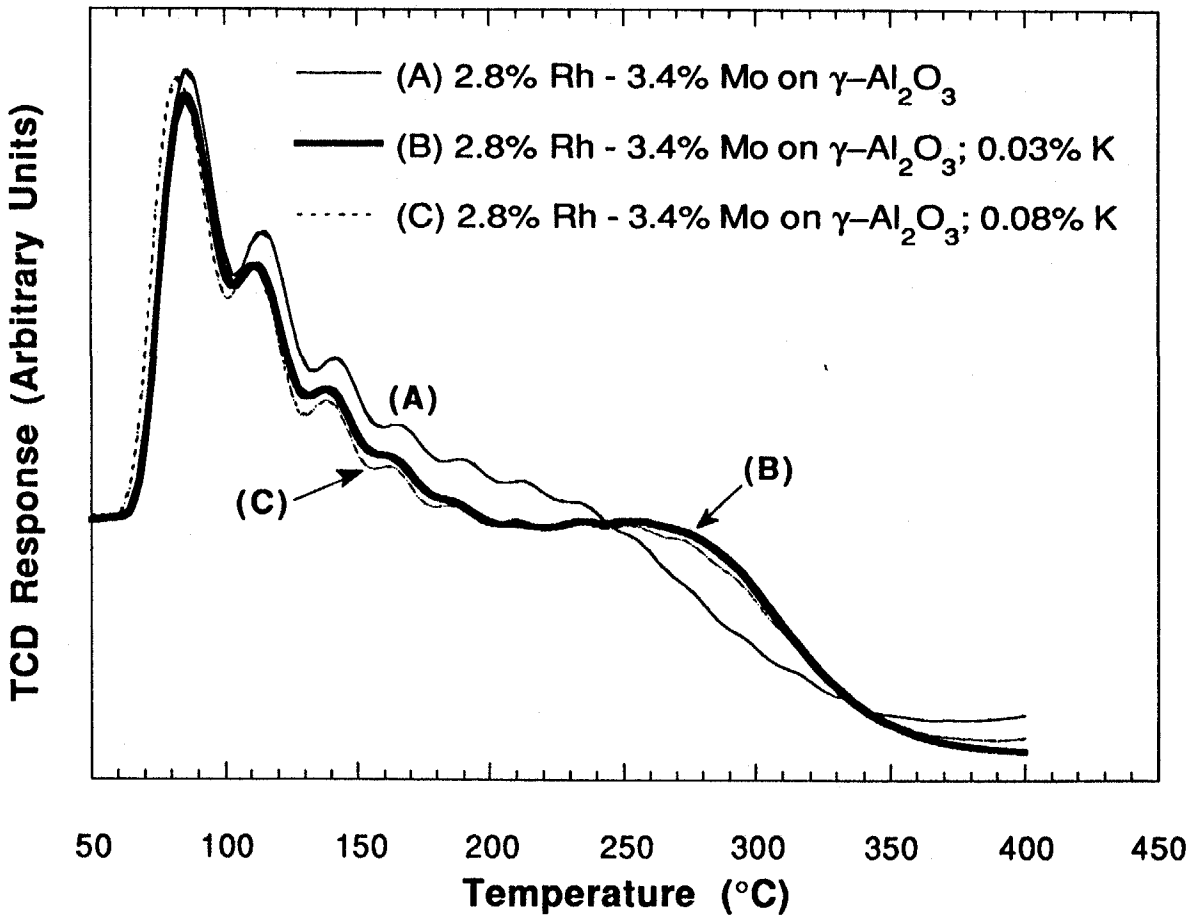

Figure 12. Ammonia Temperature Programmed Desorption for Doped Rh-Mo/γ-Al_2O_3 Series

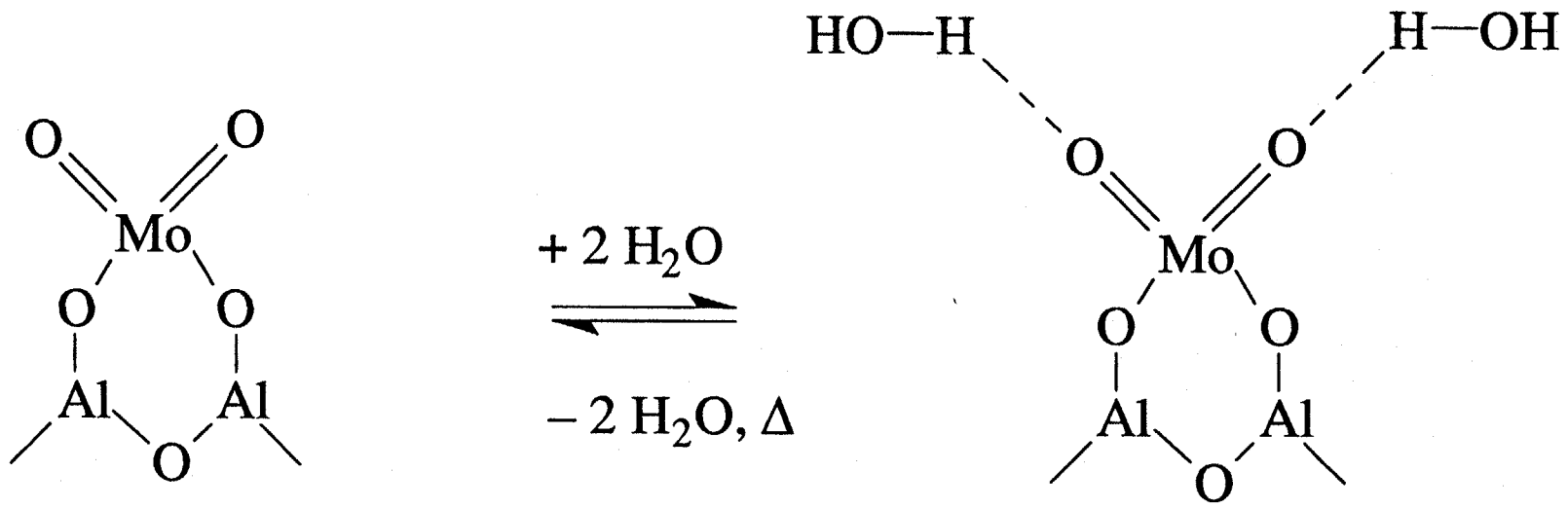

Figure 13. Mo(VI)O_4 Surface Species Adapted From Stencel, J. M. et al., *J. Catal.*, **90**, 314 (1984)